Journal of the Optical Society of America B
OPTICAL PHYSICS

Model for confined Tamm plasmon devices

Mike Adams,[1,*] Ben Cemlyn,[1] Ian Henning,[1] Matthew Parker,[2] Edmund Harbord,[2] and Ruth Oulton[2]

[1]School of Computer Science and Electronic Engineering, University of Essex, Wivenhoe Park, Colchester, CO4 3SQ, UK
[2]Quantum Engineering Technology Labs, School of Physics and Department of Electrical and Electronic Engineering, University of Bristol, 5 Tyndall Ave, Bristol BS8 1FD, UK
*Corresponding author: adamm@essex.ac.uk

Received 3 September 2018; revised 24 October 2018; accepted 8 November 2018; posted 8 November 2018 (Doc. ID 344858); published 19 December 2018

It is shown that cavities formed between a multilayer quarter-wave Bragg reflector and a metal mirror that support Tamm plasmons can be modeled by using a hard-mirror approximation, including appropriate penetration depths into the mirrors. Results from this model are in excellent agreement with those found by numerical methods. In addition, Tamm modes that are laterally confined by the presence of a metallic disk deposited on the Bragg reflector can be described by the effective index model that is commonly used for vertical-cavity surface-emitting lasers. This enables the lateral modes confined by a circular disk to be found from conventional weakly guiding waveguide theory similar to that used for optical fibers. The resonant wavelengths of these linearly polarized guided modes are calculated as functions of disk diameter and other parameters.

https://doi.org/10.1364/JOSAB.36.000125

1. INTRODUCTION

Electromagnetic modes bounded by a distributed Bragg reflector (DBR) and a metal mirror are termed Tamm plasmon-polaritons [1], or simply Tamm plasmons, by analogy to the electronic states that can appear at the surface of a crystal [2]. In the present contribution, the term "Tamm modes" will be used. Confined Tamm modes have been demonstrated with lateral confinement limited to the size of a metallic disk deposited on the DBR [3]. Lasing has been reported with Tamm modes for both large-area metal layers [4] and with confinement provided by micrometer-scale metal disks [5]. Replacing the disks by microrectangles with an aspect ratio of 2 has resulted in polarization-controlled Tamm lasers [6]. Tamm single-photon sources have been demonstrated with InGaAs/GaAs quantum dots (QDs) emitting at 910 nm [7] and InP/GaInP QDs emitting at 656 nm [8]. Other proposed device applications of Tamm modes include all-optical bistable logic [9], multichannel filters [10], and novel forms of sensors [11,12].

Analysis of one-dimensional Tamm modes is conventionally performed using the transfer matrix method (TMM; see, for example Refs. [1,4,9,12–14]). For three-dimensional confined Tamm modes, the modeling has used coupled wave analysis [5], the aperiodic Fourier modal method (a-FMM) [6], and the finite-difference time-domain (FDTD) method [3,14]. All these methods involve numerical computation and do not afford direct physical insight into modal behavior or identification of trends with variation of structural and material parameters. In the present contribution, drawing on concepts well established for modeling vertical-cavity surface-emitting lasers (VCSELs) and resonant-cavity light-emitting diodes (RCLEDs), we offer a novel approach to modeling one-dimensional and three-dimensional Tamm modes that includes all the relevant physics and offers a simpler approach to studying trends.

In the next section, the hard-mirror model for a one-dimensional cavity is applied to study Tamm modes with the aid of the concept of the penetration depth of the field into the DBR [15]. The following section extends this approach to describe three-dimensional confined Tamm plasmon modes by using the effective index model [16]. After that, a numerical example is given and compared with results from the literature where numerical methods have been used, and finally, we summarize our conclusions and the outlook for further applications of our approach.

2. ONE-DIMENSIONAL APPROXIMATION

A general one-dimensional structure to support Tamm modes is shown schematically in Fig. 1(a). It consists of a spacer layer of thickness L_S and refractive index n_S, between a multilayer quarter-wave Bragg reflector and a metal whose complex refractive index is $(n_M + ik_M)$. Figure 1(b) shows the hard-mirror

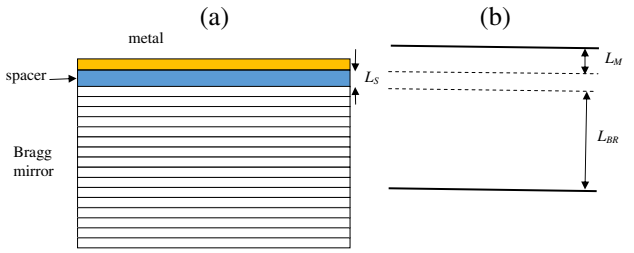

Fig. 1. (a) Schematic of one-dimensional structure to support Tamm modes; (b) equivalent hard-mirror model.

model for this cavity, allowing for penetration of the field into the DBR and the metal.

From standard VCSEL and RCLED cavity modeling (see, e.g., Refs. [17,18]), we approximate the confinement of the Tamm mode between the DBR and the metal layer as a cavity formed by two hard mirrors, each of which is positioned at a penetration depth into the appropriate medium. The penetration depths are denoted by L_M and L_{BR}, respectively, for the metal and Bragg reflector, as shown in Fig. 1(b). Rigorous expressions for the penetration depth L_{BR} are derived in Ref. [15] in terms of refractive indices, number of layers in the DBR, and wavelength. The expression for L_{BR} [see Eq. (7) below] is found from the phase delay τ_m on reflection from an m-layer quarter-wave Bragg stack. A recursion relation for τ_m is derived by adding a single quarter-wave layer to the top of an $(m-1)$-layer stack whose delay is τ_{m-1}. Full details of the derivation are given in Ref. [15]. Simpler analytical expressions that are very accurate for high numbers of layers when the penetration length saturates are given in Ref. [19]. The penetration depth into the metal, L_M, at the center (Bragg) angular frequency ω_0 of the DBR can be calculated from the phase change, β, on reflection [20]:

$$L_M = \frac{c}{2\omega_0 n_M}(\pi - \beta), \tag{1}$$

where c is the speed of light. An explicit (but lengthy) expression for $\tan\beta$ is given in Ref. [21] in terms of refractive indices, thickness of the metal, and wavelength; this expression is cast in the present notation in Appendix A. In the limit of large layer thickness, this expression reduces to the simple form obtained from the phase change on reflection from an isolated metal surface [22]. Usually β lies in the second quadrant.

The longitudinal modes of the structure occur at frequencies for which the round-trip phase is an integer multiple of 2π. Allowing also for the reflection delay τ from the Bragg mirror [15], the sum of phase terms in the cavity round trip gives

$$2\frac{\omega_N}{c}(n_S L_S + \bar{n}L_{\mathrm{BR}}) + 2\frac{\omega_0}{c}n_M L_M - \omega_0\tau = (2N-1)\pi, \tag{2}$$

where ω_N is the resonant angular frequency of mode $N(=1,2,3,\ldots)$ and the average refractive index in the Bragg mirror is defined [19] as

$$\bar{n} = \frac{n_H d_H + n_L d_L}{d_H + d_L}, \tag{3}$$

with $n_{H,L}$ and $d_{H,L}$ as the refractive indices and thicknesses of the high and low index layers in the Bragg mirror. The reason for the term $(2N-1)$ in Eq. (2) is that the combination of the spacer layer and the metal thickness should behave as a quarter-wave layer [23].

The delay time τ is related to the penetration depth in the DBR by

$$\tau = \frac{2\bar{n}}{c}L_{\mathrm{BR}}. \tag{4}$$

Using Eq. (4), Eq. (2) can be rewritten in the form

$$\frac{\omega_N}{c}n_S L_S + \frac{\omega_0}{c}n_M L_M + \frac{(\omega_N - \omega_0)}{c}\bar{n}L_{\mathrm{BR}} = \left(N - \frac{1}{2}\right)\pi. \tag{5}$$

Equation (5) is the cavity resonance condition in terms of the phase changes in the spacer and on reflection from the metal and the DBR. It shows explicitly that when the mode frequency occurs at the center frequency of the grating, there is no dependence on the penetration depth L_{BR}. This is because in this case the phase on reflection from the grating is either zero or π. Equation (5) here is equivalent to Eq. (5) in Ref. [1], with the difference that in Ref. [1], the refractive index of the metal is given by the Drude model, and there is no spacer layer ($L_S = 0$).

From Eq. (5), it follows that the mode frequency ω_N is given by

$$\omega_N = \frac{\omega_0(\bar{n}L_{\mathrm{BR}} - n_M L_M) + c\pi\left(N - \frac{1}{2}\right)}{n_S L_S + \bar{n}L_{\mathrm{BR}}}. \tag{6}$$

From Ref. [15], the expression for L_{BR} is

$$L_{\mathrm{BR}} = \frac{\pi c}{2\omega_0\bar{n}}\frac{q}{1-p}\frac{(1-a^2p^{m-1})(1-p^m)}{(1-q^2a^2p^{2m-2})}, \tag{7}$$

where m is the number of layers in the DBR and a, p, q are refractive index ratios (low to high) of the three types of interfaces that characterize the mirror:

$$a = \frac{n_{\mathrm{LE}}}{n_{\mathrm{HE}}}p = \frac{n_L}{n_H}q = \frac{n_{\mathrm{LI}}}{n_{\mathrm{HI}}}. \tag{8}$$

The ratio a applies to the interface between the last DBR layer and the exit medium (subscript E), and the ratio q refers to the interface between the incident medium (subscript I) and the first DBR layer. We note here that the simpler expressions for penetration depth [15,19] are not sufficiently accurate for the numerical example considered below because the index differences are too large.

In the numerical work below, the full expression [21] for the phase β will be used in Eq. (1) for the penetration depth of the metal in order to include the effect of a finite layer.

3. THREE-DIMENSIONAL APPROXIMATION

To model confinement in the lateral direction, we follow the effective index approach proposed in Ref. [16] and now widely used for VCSEL design. The essence of this method is that the lateral effective index profile is determined by the local changes of the Fabry–Perot cavity resonance wavelength. So, for a

circular metal disk on top of the vertical structure discussed above, the change of effective index, Δn_e, is related to the change of resonant wavelength, $\Delta\lambda$, by

$$\frac{\Delta n_e}{n_e} = \frac{\Delta\lambda}{\lambda}, \tag{9}$$

where n_e is the effective index of the cavity given by the mean value of indices in the spacer and the Bragg mirror:

$$n_e L_{\text{eff}} = n_S L_S + \bar{n} L_{\text{BR}}, \tag{10}$$

with the total effective cavity length, L_{eff}, defined as

$$L_{\text{eff}} = L_S + L_{\text{BR}}. \tag{11}$$

The resulting radial index profile is illustrated in Fig. 2(a), with a schematic of the physical structure in Fig. 2(b).

For the region outside that beneath the metal disk, the upper mirror of the effective Fabry–Perot cavity is formed by the semiconductor-air interface. Hence in this region, Eq. (5) is replaced by

$$\frac{\omega_{Nc}}{c} n_S L_S + \frac{(\omega_{Nc} - \omega_0)}{c} \bar{n} L_{\text{BR}} = \pi\left(N - \frac{1}{2}\right), \tag{12}$$

where ω_{Nc} is the mode frequency in this region. It follows that the quantity $\Delta\lambda$, required in Eq. (9), is given by

$$\Delta\lambda = 2\pi c\left(\frac{1}{\omega_N} - \frac{1}{\omega_{Nc}}\right). \tag{13}$$

Thus, solutions of Eqs. (5) and (12) can be used in Eqs. (9) and (13) to calculate the effective index profile in the radial direction.

The resulting circular waveguide of diameter d, core index n_e, and core-cladding index difference $\Delta n_e (\ll n_e)$ supports modes that are, to a very good approximation, linearly polarized (LP) by analogy with the modes of weakly guiding optical fibers [24]. These LP modes are characterized by the index eigenvalues, n, of the wave equation such that their cutoff frequency is given by $n = n_e - \Delta n_e$. These modes are characterised by two subscripts, one for each of the radial and azimuthal coordinates. We will use l as the azimuthal subscript and p as the radial subscript, so that the mode is labeled LP_{lp}. Mode solver software for the LP modes is widely available for optical fibers and can simply be used for the corresponding confined Tamm modes with appropriate definitions of core and cladding indices, as described above.

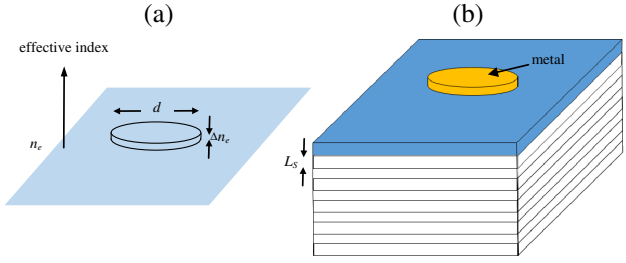

Fig. 2. (a) Effective index model of circularly symmetric cylindrical waveguide for the three-dimensional structure to support confined Tamm modes shown in (b).

Assuming the solutions for n have been found, the frequency of the confined mode, ω_{lp}, can be calculated by using again the cavity resonance condition in the form:

$$\omega_{lp} = \frac{\omega_0(\bar{n} L_{\text{BR}} - n_M L_M) + c\pi\left(N - \frac{1}{2}\right)}{n L_{\text{eff}}}. \tag{14}$$

Equation (14) indicates that the confined Tamm resonant wavelength is directly proportional to the index eigenvalue for the corresponding LP mode.

4. NUMERICAL EXAMPLE

The method outlined above will be illustrated by applying it to the structure designed for Tamm modes in Ref. [14], which has a GaAs spacer, an AlAs/GaAs DBR with 35 layers, and a GaAs substrate. Hence the incident and exit media have the same (high) refractive index [25], and the first and last layers of the DBR have the same (low) index [26]. The metal is gold with $n_M = 0.38$ and $k_M = 8.7$ in the wavelength range of interest [27]. Numerical values of the semiconductor parameters are given in Table 1. The stopband of the Bragg mirror lies between 1205 and 1375 nm [14], so this defines the value of the Bragg frequency.

Figure 3 shows the variation of phase with thickness of the gold layer calculated using the expression in Ref. [21].

Using Eq. (6) with $N = 1$ for a 25 nm gold thickness and 75 nm spacer gives $\omega_1 = 1.4487 \times 10^{15}$ rad/s, corresponding to a Tamm wavelength of 1301.1 nm. This compares well with the value of 1304 nm reported for this structure in Ref. [14], where the TMM was used. It is interesting also to estimate the Tamm resonance from the approximation used in Ref. [1],

Table 1. Semiconductor Parameter Values

λ_0 (nm)	1284.4
$\omega_0 (\times 10^{15}$ rad/s)	1.4676
$n_S, n_H, n_{\text{HI}}, n_{\text{HE}}$	3.409
$n_L, n_{\text{LI}}, n_{\text{LE}}$	2.910
p, q, a	0.854
d_H (nm)	94.2
d_L (nm)	110.4
$\bar{n}$	3.139
L_{DBR} (nm)	591.9

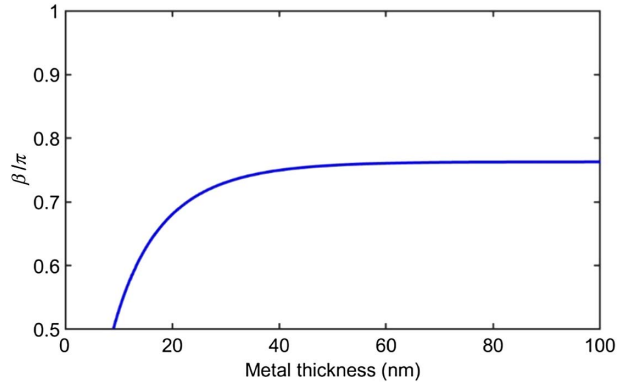

Fig. 3. Phase on reflection from metal (gold) versus thickness.

where the Drude model for the metal is used. Adapting the result from Ref. [1] to allow for the presence of a spacer layer gives

$$\omega_1 = \frac{\omega_0\left(1+\frac{\Delta n}{2n_H}\right)}{1+\frac{\omega_0\Delta n}{\pi}\left(\frac{2}{\omega_p\sqrt{\varepsilon_b}}+\frac{n_S L_S}{n_H c}\right)}, \tag{15}$$

where $\Delta n = n_H - n_L, \omega_p$ is the plasma frequency, and ε_b is the background dielectric constant. Using our parameter values in Eq. (15) with a plasma energy of 8.9 eV [1] yields a frequency of 1.441×10^{15} rad/s, corresponding to a Tamm wavelength of 1308 nm. This level of agreement may be fortuitous, since the approximation in Eq. (15) takes no account of the gold thickness nor of the number of layers in the Bragg mirror, effectively assuming both these quantities are approaching infinity. Since the penetration depth into the DBR is approaching saturation for 35 layers, we do not expect additional layers to affect the resonant wavelength from Eq. (6) significantly. However, it is clear from Fig. 3 that the phase on reflection from the mirror is some way from saturation at a thickness of 25 nm, and hence, a change of the Tamm wavelength is expected, as we demonstrate below.

Figure 4 shows the Tamm resonance wavelength as a function of (a) spacer thickness with the gold thickness constant at 25 nm, and (b) gold thickness with the spacer thickness kept constant at 75 nm. Results from the present model are compared with those from the TMM [14], and again the agreement is very good. The small departures between the two are attributed to inclusion of the dispersion of the refractive indices in the TMM.

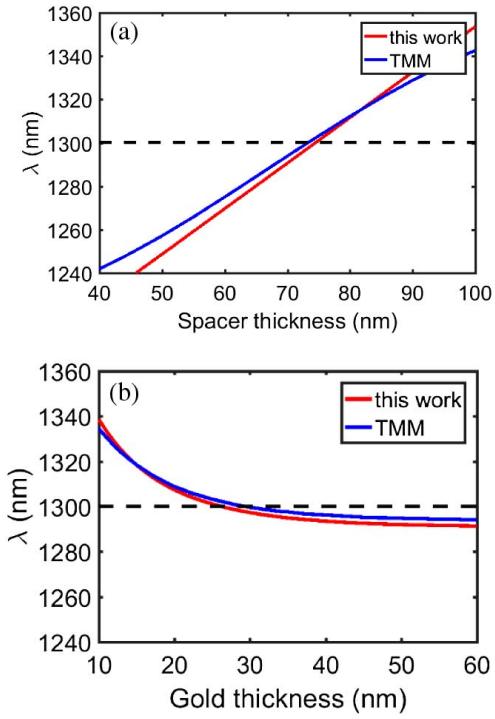

Fig. 4. Calculated Tamm wavelength (a) versus spacer thickness for fixed gold thickness of 25 nm, and (b) versus gold thickness for fixed spacer thickness for 75 nm.

Table 2. Cutoffs of LP Modes

LP Mode	Equivalent Modes	d_c (μm)
LP_{01}	HE_{11}	0
LP_{11}	$HE_{21}, TE_{01}, TM_{01}$	1.10
LP_{02}, LP_{21}	$HE_{12}, EH_{11}, HE_{31}$	1.72
LP_{31}	EH_{21}, HE_{41}	2.30
LP_{12}	$HE_{22}, TE_{02}, TM_{02}$	2.47
LP_{41}	EH_{41}, HE_{51}	2.86
LP_{03}, LP_{22}	$HE_{13}, EH_{12}, HE_{32}$	3.14
LP_{51}	EH_{41}, HE_{61}	3.40
LP_{32}	EH_{23}, HE_{42}	3.77
LP_{13}	$HE_{23}, TE_{03}, TM_{03}$	3.88
LP_{61}	EH_{51}, HE_{71}	3.93

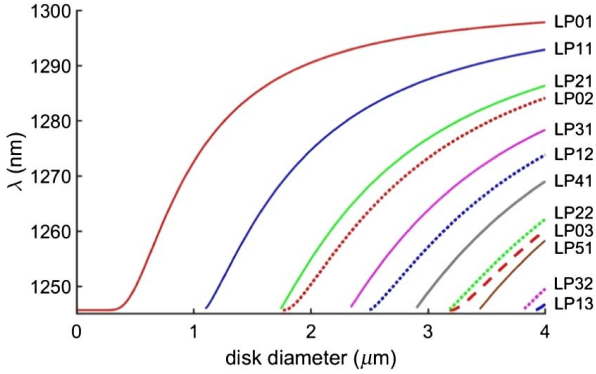

Fig. 5. Calculated Tamm wavelength for the first 12 LP modes versus disk diameter for gold thickness 25 nm and spacer thickness 75 nm.

Turning to the two-dimensional model, for the case of a 75 nm spacer and 25 nm of gold, in the region outside that beneath the metal disk, Eq. (12) is used with $N = 1$ to calculate a wavelength of 1245.8 nm. Hence, we can use Eq. (9) with $\lambda = 1307.7$ nm, $\Delta\lambda = 55.3$ nm, and $n_e = 3.170$ [from Eq. (10)] to calculate the value of Δn_e as 0.135. For these parameter values, the cutoff values (d_c) of the disk diameter for the LP modes can be calculated. Table 2 gives the values of d_c for some lower-order LP modes using the effective index and index difference values calculated for this example. Each LP mode corresponds to hybrid (HE or EH), transverse electric (TE), or transverse magnetic (TM) modes, as indicated in Table 2. More details of these waveguide modes are given in many textbooks; see, for example, [28,29]. Mode profiles are illustrated in several good tutorial websites; see, for example, [30,31]. The number of lateral modes increases rapidly with disk diameter. Single-mode operation is only found for a diameter less than 1.1 μm.

The calculated variation of resonant wavelength with disk diameter, using Eq. (14) for the first 12 LP modes, is shown in Fig. 5. The trends here are similar to those measured and calculated in Ref. [3] (albeit expressed there in terms of photon energy rather than wavelength) for a somewhat similar structure.

5. CONCLUSION

We have shown that concepts widely used in design and analysis of VCSELs and RCLEDs can be successfully applied to model Tamm modes confined between a metal layer and a Bragg reflector. The hard-mirror approach, where an effective cavity is defined to include penetration depths of the optical wave into the metal and the Bragg mirror, successfully predicts the resonant wavelengths of one-dimensional Tamm modes. It is worth noting that this approach uses the calculated phase on reflection from the metal, using measured real and imaginary parts of the refractive index rather than invoking the Drude model. Three-dimensional Tamm modes can be modeled using the effective index approach, where the radial effective index profile is found from the difference in resonant wavelengths between the one-dimensional mode beneath a circular metal disk and that outside this region. This enables the number of transverse modes and their wavelengths to be determined as functions of disk diameter and other parameters, a task which is not straightforward with purely numerical computational approaches.

It is clear that the methods proposed here can be applied to a wider range of structures than those currently of interest. While attention has been confined here to circular disks, the method proposed could just as well be applied to disks of other shapes, e.g., elliptical, racetrack, or rectangular, since the basic principle of decoupling the vertical field component from the lateral components applies independently of the geometry. Thus, for example, the method could be used to study polarization properties of noncircularly symmetric disks, such as the microrectangles used in Ref. [6], or more complicated shapes of the metal layer. In this context, it is worth noting that approximate but accurate solutions are available for some shapes, such as elliptical [32] or rectangular [33]. Further developments could include analysis of the effects of metallic layers and/or spacers of differing thicknesses in the lateral directions, thus opening up the prospect of integrating novel Tamm modal devices on a single Bragg mirror in order to produce multifunctional components for a variety of potential applications.

APPENDIX A: EXPRESSION FOR THE PHASE CHANGE, β, ON REFLECTION FROM A METAL

For a wave of wavelength λ incident from the spacer (refractive index n_S) on a metal of complex refractive index $(n_M + ik_M)$ and thickness L_M, with air (refractive index 1) on the other side, the expression for $\tan\beta$ is [21]

$$\tan\beta = \frac{\left\{\begin{array}{l} 2n_S k_M[k_M^2 + (n_M+1)^2]\exp(4\pi k_M L_M/\lambda) - 2n_S k_M[k_M^2 + (n_M-1)^2]\exp(-4\pi k_M L_M/\lambda) \\ -8n_S n_M k_M \cos(4\pi n_M L_M/\lambda) - 4n_S n_M(k_M^2 + n_M^2 - 1)\sin(4\pi n_M L_M/\lambda) \end{array}\right\}}{\left\{\begin{array}{l} [k_M^2(n_S^2-1) + n_S^2(n_M+1)^2 - (k_M^2 + n_M^2 + n_M)^2]\exp(4\pi k_M L_M/\lambda) \\ +[k_M^2(n_S^2-1) + n_S^2(n_M-1)^2 - (k_M^2 + n_M^2 - n_M)^2]\exp(-4\pi k_M L_M/\lambda) \\ +2[n_S^2(k_M^2 + n_M^2 - 1) + (k_M^2 + n_M^2 - n_M)(k_M^2 + n_M^2 + n_M) - k_M^2]\cos(4\pi n_M L_M/\lambda) \\ -4k_M(k_M^2 + n_M^2 + n_S^2)\sin(4\pi n_M L_M/\lambda) \end{array}\right\}}.$$

Funding. Engineering and Physical Sciences Research Council (EPSRC) (EP/G012458/1, EP/M024156/1, EP/M024237/1, EP/N003381/1).

REFERENCES

1. M. Kaliteevski, I. Iorsh, S. Brand, R. A. Abram, J. M. Chamberlain, A. V. Kavokin, and I. A. Shelykh, "Tamm plasmon-polaritons: possible electromagnetic states at the interface of a metal and a dielectric Bragg mirror," Phys. Rev. B **76**, 165415 (2007).
2. I. E. Tamm, "O vozmozhnoi sviazi elektronov na poverkhnostiakh kristalla," Zh. Eksp. Teor. Fiz. **3**, 34–35 (1933) (in Russian).
3. O. Gazzano, S. Michaelis de Vasconcellos, K. Gauthron, C. Symonds, J. Bloch, P. Voisin, J. Bellessa, A. Lemaître, and P. Senellart, "Evidence for confined Tamm plasmon modes under metallic microdisks and application to the control of spontaneous optical emission," Phys. Rev. Lett. **107**, 247402 (2011).
4. C. Symonds, A. Lemaître, P. Senellart, M. H. Jomaa, S. Aberra Guebrou, E. Homeyer, G. Brucoli, and J. Bellessa, "Lasing in a hybrid GaAs/silver Tamm structure," Appl. Phys. Lett. **100**, 121122 (2012).
5. C. Symonds, G. Lheureux, J. P. Hugonin, J. J. Greffet, J. Laverdant, G. Brucoli, A. Lemaître, P. Senellart, and J. Bellessa, "Confined Tamm plasmon lasers," Nano Lett. **13**, 3179–3184 (2013).
6. G. Lheureux, S. Azzini, C. Symonds, P. Senellart, A. Lemaître, C. Sauvan, J.-P. Hugonin, J.-J. Greffet, and J. Bellessa, "Polarization-controlled confined Tamm plasmon lasers," ACS Photon. **2**, 842–848 (2015).
7. O. Gazzano, S. Michaelis de Vasconcellos, K. Gauthron, C. Symonds, P. Voisin, J. Bellessa, A. Lemaître, and P. Senellart, "Single photon source using confined Tamm plasmon modes," Appl. Phys. Lett. **100**, 232111 (2012).
8. T. Braun, V. Baumann, O. Iff, S. Höfling, C. Schneider, and M. Kamp, "Enhanced single photon emission from positioned InP/GaInP quantum dots coupled to a confined Tamm-plasmon mode," Appl. Phys. Lett. **106**, 041113 (2015).
9. W. L. Zhang, Y. Jiang, Y. Y. Zhu, F. Wang, and Y. J. Rao, "All-optical bistable logic control based on coupled Tamm plasmons," Opt. Lett. **38**, 4092–4095 (2013).
10. H. Zhou, G. Yang, K. Wang, H. Long, and P. Lu, "Multiple optical Tamm states at a metal–dielectric mirror interface," Opt. Lett. **35**, 4112–4114 (2010).
11. B. Auguié, M. C. Fuertes, P. C. Angelomé, N. L. Abdala, G. S. Illia, and A. Fainstein, "Tamm plasmon resonance in mesoporous multilayers: toward a sensing application," ACS Photon. **1**, 775–780 (2014).
12. W. L. Zhang, F. Wang, Y. J. Rao, and Y. Jiang, "Novel sensing concept based on optical Tamm plasmon," Opt. Express **22**, 14524–14529 (2014).
13. M. E. Sasin, R. P. Seisyan, M. A. Kalitteevski, S. Brand, R. A. Abram, J. M. Chamberlain, A. Y. Egorov, A. P. Vasil'ev, V. S. Mikhrin, and A. V. Kavokin, "Tamm plasmon polaritons: slow and spatially compact light," Appl. Phys. Lett. **92**, 251112 (2008).
14. M. Parker, E. Harbord, A. Young, P. Androvitsaneas, J. Rarity, and R. Oulton, "Tamm plasmons for efficient interaction of telecom wavelength photons and quantum dots," IET Optoelectron. **12**, 11–14 (2018).

15. D. I. Babic and S. W. Corzine, "Analytic expressions for the reflection delay, penetration depth, and absorptance of quarter-wave dielectric mirrors," IEEE J. Quantum Electron. **28**, 514–524 (1992).
16. G. R. Hadley, "Effective index model for vertical-cavity surface-emitting lasers," Opt. Lett. **20**, 1483–1485 (1995).
17. R. Michalzik, "VCSEL fundamentals," in *VCSELs. Fundamentals, Technology and Applications of Vertical-Cavity Surface-Emitting Lasers*, R. Michalzik, ed. (Springer, 2013), pp. 19–75.
18. D. Delbeke, R. Bockstaele, P. Bienstman, R. Baets, and H. Benisty, "High-efficiency semiconductor resonant-cavity light-emitting diodes: a review," IEEE J. Sel. Top. Quantum Electron. **8**, 189–206 (2002).
19. L. R. Brovelli and U. Keller, "Simple analytical expressions for the reflectivity and the penetration depth of a Bragg mirror between arbitrary media," Opt. Commun. **116**, 343–350 (1995).
20. F. Ma and X. Liu, "Phase shift and penetration depth of metal mirrors in a microcavity structure," Appl. Opt. **46**, 6247–8250 (2007).
21. J. M. Bennett, "Precise method for measuring the absolute phase change on reflection," J. Opt. Soc. Am. **54**, 612–624 (1964).
22. W. Lichten, "Precise wavelength measurements and optical phase shifts. I. General theory," J. Opt. Soc. Am. A **2**, 1869–1876 (1985).
23. Z. Zhang, K. Torizuka, T. Itatani, K. Kobayashi, T. Sugaya, T. Nakagawa, and H. Takahashi, "Broadband semiconductor saturable-absorber mirror for a self-starting mode-locked Cr: forsterite laser," Opt. Lett. **23**, 1465–1467 (1998).
24. D. Gloge, "Weakly guiding fibers," Appl. Opt. **10**, 2252–2258 (1971).
25. T. Skauli, P. S. Kuo, K. L. Vodopyanov, T. J. Pinguet, O. Levi, L. A. Eyres, J. S. Harris, M. M. Fejer, B. Gerard, L. Becouarn, and E. Lallier, "Improved dispersion relations for GaAs and applications to nonlinear optics," J. Appl. Phys. **94**, 6447–6455 (2003).
26. R. E. Fern and A. Onton, "Refractive index of AlAs," J. Appl. Phys. **42**, 3499–3500 (1971).
27. P. B. Johnson and R. W. Christy, "Optical constants of the noble metals," Phys. Rev. B **6**, 4370–4379 (1972).
28. M. J. Adams, *An Introduction to Optical Waveguides* (Wiley, 1981), Chap. 7.
29. A. W. Snyder and J. D. Love, *Optical Waveguide Theory* (Chapman and Hall, 1983), Chap. 14.
30. Fiber Optics for Sale Co., "Basic optics for optical fiber," https://www.fiberoptics4sale.com/blogs/archive-posts/95048070-basic-optics-for-optical-fiber.
31. R. Paschotta, "Encyclopedia of laser physics and technology," https://www.rp-photonics.com/lp_modes.html.
32. R. B. Dyott, *Elliptical Fiber Waveguides* (Artech House, 1995).
33. E. Marcatili, "Dielectric rectangular waveguide and directional coupler for integrated optics," Bell Syst. Tech. J. **48**, 2071–2102 (1969).